Cement & Concrete Composites 34 (2012) 208–217

Contents lists available at SciVerse ScienceDirect

Cement & Concrete Composites

journal homepage: www.elsevier.com/locate/cemconcomp

Numerical simulation of the variation of fiber orientation distribution during flow molding of Ultra High Performance Cementitious Composites (UHPCC)

Su-Tae Kang [a,*], Jin-Keun Kim [b,1]

[a] Department of Civil Engineering, Daegu University, 201, Daegudae-ro, Jillyang, Gyeongsan, Gyeongbuk 712-714, South Korea
[b] Department of Civil and Environmental Engineering, Korea Advanced Institute of Science and Technology (KAIST), 373-1, Guseong-dong, Yuseong-gu, Daejeon 305-701, South Korea

ARTICLE INFO

Article history:
Received 24 June 2010
Received in revised form 18 September 2011
Accepted 21 September 2011
Available online 29 September 2011

Keywords:
Fiber orientation
Flow molding
Numerical analysis
High performance concrete
Shear flow
Radial flow

ABSTRACT

In this paper, the variation of the fiber orientation distribution along the flow of fresh UHPCC was studied. In order to describe the rotational motion of a single fiber, Jeffery's equation was adopted, in which the interaction among fibers is neglected. Two cases of flow patterns were considered: shear flow and radial flow. Starting with a three-dimensional random distribution of fibers, the fiber orientation distribution along the flow distance was simulated. These results reveal that fibers gradually become more parallel (in the case of shear flow) and perpendicular (in the case of radial flow) to the flow direction as the flow distance increases. This approach will be useful to predict flow-dependent tensile behavior considering the change of fiber orientation distribution.

1. Introduction

Ultra High Performance Cementitious Composites (UHPCC) are composed of fine particles, smaller than 0.5 mm, and without coarse aggregate [1]. By optimizing the granular mixture in order to maximize the density, UHPCC presents very high compressive strengths of more than 200 MPa. However, as is well known, cementitious materials of higher strength tend to be more brittle. Therefore, UHPCC includes fibers to ensure sufficient ductility and energy absorption capacity. Several types of fibers have been incorporated into UHPCC, and one of the most commonly used is straight steel fiber (with a length of 13 mm, diameter of 0.2 mm, and tensile strength of 2500 MPa).

The most important advantages of adopting fibers within UHPCC are the improvements of tensile strength and toughness. However, these properties are strongly influenced by fiber orientation distribution along the direction of tensile loading [2–4].

Various shapes of fibers with different length and diameter are used for fiber reinforced concrete. These fibers are often assumed to be dispersed randomly in all directions so as to exhibit isotropic behavior. However, the real fiber orientation distribution can be strongly influenced by various factors such as fiber characteristics (diameter, length, volume fraction, etc.), the fluidity of the matrix, placing method, shape and dimensions of the forms, etc.

The high viscosity and fluidity of UHPCC make the fiber orientation distribution more dependent on the flow characteristics, which in turn are determined by factors such as the casting sequence, shape of the structure, etc. Consequently, the flow-induced orientation distribution of fibers not only influences mechanical properties and structural performance but also makes it necessary to treat UHPCC as an anisotropic material.

Research on fiber orientation or dispersion has been carried out since the early 1970s [5–7]. However, this field was mostly approached in terms of the mechanics of composite materials, whereas few studies were carried out in terms of fluid mechanics [8].

If the change of the fiber orientation distribution along the flow of fluid can be predicted, it becomes possible to enhance the structural performance effectively by utilizing the anisotropy of UHPCC, and also to considerably reduce the performance instability that may arise in a structure when the fiber orientation is not controlled. Accordingly, efficient as well as reliable structural design and construction may be achieved.

This paper presents a means for predicting the variation of the fiber orientation distribution along the flow of fresh UHPCC. To this end, it is first necessary to understand the flow field in the placing process of a viscous fluid such as mortar and to study the relation between the flow field and the fiber orientation.

* Corresponding author. Tel.: +82 53 850 6528; fax: +82 53 850 6529.
E-mail addresses: stkang@daegu.ac.kr (S.-T. Kang), kimjinkeun@kaist.ac.kr (J.-K. Kim).
[1] Tel.: +82 42 350 3614; fax: +82 42 350 3688.

0958-9465/$ - see front matter © 2011 Elsevier Ltd. All rights reserved.
doi:10.1016/j.cemconcomp.2011.09.015

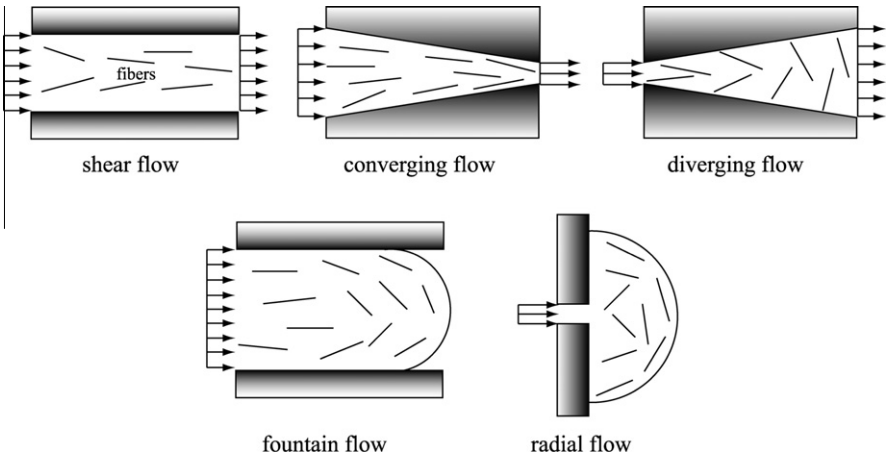

Fig. 1. Short fiber orientation in various flow fields.

As mentioned earlier, during the flow molding process, the flow field of cementitious mortar is strongly influenced by various factors: the geometric shape of the form, the placing process conditions (such as position and direction), mortar rheology [9,10], etc. The flow fields that can occur during the flow molding process of viscous fluids are generally classified as shown in Fig. 1.

In order to predict the flow field and the corresponding fiber orientation distribution, a numerical simulation is required for the entire domain. However, since three-dimensional flow analyses are complicated, two-dimensional analyses are often conducted in either the plane or thickness directions. In this study, planar flow analysis is carried out for UHPCC and the consequent variation of the fiber orientation distribution is estimated.

2. Theory and analytical modeling

2.1. Flow kinematics and fiber orientation

Few studies to predict the variation of the fiber orientation along the fluid flow have been reported for fiber reinforce concrete, but there has been a wealth of research in the field of flow molding of short fiber reinforced polymers [11–19]. Thermoplastic polymers are normally considered as a viscoelastic fluid. Most researches related to the fiber orientation in the flow molding process of short fiber reinforced polymer find their origins in Jeffery [20].

In 1922, Jeffery [20] derived an equation of orientation change of an ellipsoidal particle immersed in a homogeneous flow field based on hydrodynamics. In 1970, Batchelor [11] developed a generalized equation for the hydrodynamic stress for a slender-body, i.e. a suspension of long axisymmetric rigid particle. Dinh and Armstrong [21], extending Batchelor's approach and using Jeffery's equation, have developed a constitutive equation for semi-concentrated suspensions of rigid fibers with an infinite aspect ratio (L_f/D_f) in a Newtonian fluid undergoing homogeneous flow. Ausias el al. [12], using a similar approach to Dinh and Armstrong [21], developed a model for dilute suspensions of long rigid fibers and extended it to concentrated suspensions.

Folgar and Tucker [22] proposed a model for the orientation behavior of fibers in concentrated suspensions of fibers. They added a diffusion term to Jeffery's equation in order to take into account the interaction among fibers.

Describing the orientation of individual fibers is ineffective, however, because composites contain numerous short fibers. Thus, the concept of a probabilistic orientation distribution function needs to be introduced to fully describe the distribution of the fiber orientation. Dinh and Armstrong [21] derived an analytical solution for an orientation distribution function applicable to a homogeneous flow field. Advani and Tucker [23] introduced the orientation tensor as well as the orientation distribution function to describe the fiber orientation more effectively.

2.2. Description of fiber orientation distribution

In order to express the orientation distribution of fibers, first of all, it needs to define the orientation of a single fiber. The fibers are assumed to be rigid cylinders, uniform in length and diameter. The orientation of the single fiber can be described as a unit vector $\bar{p}$ directed along its axis, with θ and ϕ in the spherical coordinate system, as shown in Fig. 2. The components of vector $\bar{p}$ in the cartesian coordinate system are then evidently given as functions of θ and ϕ.

$$\begin{aligned} p_1 &= \sin\theta\cos\phi \\ p_2 &= \sin\theta\sin\phi \\ p_3 &= \cos\theta \end{aligned} \tag{1}$$

The main concern is not to describe the orientation of individual fiber but the orientation distribution of all fibers since fiber reinforced composites contains numerous short fibers. Thus, the concept of probabilistic distribution is introduced to fully describe the distribution of fiber orientation in three dimensions. The orientation distribution function (ODF) ψ is first introduced. The orientation distribution function, which gives the probability of a fiber having an orientation $\bar{p}$ at the time t, is the most basic, general, and complete description of fiber orientation state. The probability of a fiber with the angle θ between θ_o and $\theta_o + d\theta$ as well as the angle ϕ between ϕ_o and $\phi_o + d\phi$ is as follows:

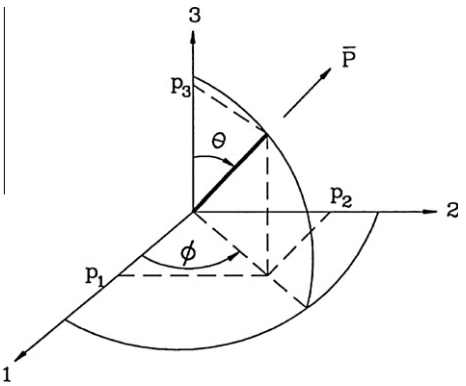

Fig. 2. Coordinate system to define the fiber orientation.

$$P_r(\theta_o \leqslant \theta \leqslant \theta_o + d\theta,\ \phi_o \leqslant \phi \leqslant \phi_o + d\phi) = \psi(\theta,\phi)\sin\theta_o\, d\theta_o\, d\phi \quad (2)$$

The orientation distribution function should satisfy the following two conditions. The first is the periodic condition that has a period of π.

$$\psi(\theta,\phi) = \psi(\pi-\theta,\pi+\phi) \quad \text{or} \quad \psi(\bar{p}) = \psi(-\bar{p}) \quad (3)$$

The second is the normalization condition, so the integral of ψ over all orientation space must be unit.

$$\int_{\theta=0}^{\theta=\pi}\int_{\phi=0}^{\phi=2\pi}\psi(\theta,\phi)\sin\theta\, d\theta\, d\phi = 1 \text{ or } \oint \psi(\bar{p})d\bar{p} = 1 \quad (4)$$

2.3. Flow and fiber orientation

For description of the motion of a single fiber, the governing equation can be represented by the following equation [22].

$$\dot{p}_i = -\frac{1}{2}\omega_{ij}p_j + \frac{1}{2}\lambda(\dot{\gamma}_{ij}p_j - \dot{\gamma}_{kl}p_k p_l p_i) - \frac{D_r}{\psi}\frac{\partial\psi}{\partial p_i} \quad (5)$$

where ω_{ij} represents the component of vorticity and $\dot{\gamma}_{ij}$ means the component of shear strain rate. They are defined as Eqs. (6) and (7), respectively.

$$\omega_{ij} = \frac{\partial V_j}{\partial x_i} - \frac{\partial V_i}{\partial x_j} \quad (6)$$

$$\dot{\gamma}_{ij} = \frac{\partial V_j}{\partial x_i} + \frac{\partial V_i}{\partial x_j} \quad (7)$$

V_i indicates the velocity component, and λ is a shape factor being related to the aspect ratio of fiber ($r_e = L_f/D_f$), given by the following.

$$\lambda = \frac{r_e^2 - 1}{r_e^2 + 1} \quad (8)$$

As can be seen, it attains values between 0 (for sphere) and 1 (for infinitely slender) depending on the aspect ratio of fiber. D_r is the rotary diffusivity that accounts for interaction among fibers. Without this term, Eq. (5) becomes identical to Jeffery's equation [20].

Folgar and Tucker [22] proposed the relation of $D_r = C_I\dot{\gamma}$, in which C_I is fiber–fiber interaction coefficient depending on the fiber geometry and volume fraction, and can be obtained through experiments. $\dot{\gamma}$ is an effective shear rate, given by the equation of $\dot{\gamma} = \sqrt{(\dot{\gamma}_{ij}\dot{\gamma}_{ij})/2}$.

2.4. Probability density function of fiber orientation

Probability Density Function (PDF), P_r is defined as the following.

$$P_r(\theta,\phi) = \psi(\theta,\phi)\sin\theta\, d\theta\, d\phi \quad (9)$$

At $t = 0$, if it is assumed that the fibers are initially randomly oriented in three dimensions, the initial orientation distribution function ψ has a value of $\psi(\theta,\phi) = 1/4\pi$.

The fiber orientation varies from initial value of (θ,ϕ) to (θ',ϕ') during a certain time interval. And thus the orientation distribution function also varies from $\psi(\theta,\phi)$ to $\psi(\theta',\phi')$. Accordingly, the probability density function, expressed as a function of time, can be written as the following.

$$P_r(\theta',\phi',t) = \psi(\theta',\phi',t)\sin\theta\, d\theta\, d\phi \quad (10)$$

From $P_r(\theta',\phi',t)$ at a time t, the variation of the fiber orientation distribution in a flow can be predicted.

3. Prediction of fiber orientation distribution in shear flow

3.1. Analysis conditions

Here, a process of manufacturing a rectangular UHPCC beam is considered, and we attempt to predict the variation of the fiber orientation distribution as fresh UHPCC flows. The beam was assumed to have dimensions of 180 mm width, 270 mm depth, and 2900 mm length, respectively. Fibers with 13 mm length and 0.2 mm diameter are considered. In order to apply the numerical solution of the flow field, the flow was assumed as a shear flow between infinite parallel plates in a steady state.

In fully developed shear flow between infinite parallel plates, there is only a component of velocity in the flow direction but no component in the other directions. That is, assuming the flow direction is defined as x direction in Cartesian coordinate system, $V_x \neq 0$ and $V_y = V_z = 0$. Furthermore, since the flow was assumed to be fully developed, the velocity is constant regardless of the flow distance and, hence, depends on y only, so that $V_x = V_x(y)$ and the velocity profile has parabolic form. The velocity profile can be applied for Newtonian fluid as well as Bingham fluid in fluid dynamics. As already well known, mortar or concrete can be commonly classified as Bingham fluid.

The flow volume rate in the inlet, Q was assumed to be 0.001 m^3/s considering the flow rate under practicable placement conditions. It is necessary to assume a value for the depth of the flow so as to regard it as a two-dimensional planar flow, where the depth depends on the kind and characteristics of the flow. For example, a fluid with low viscosity like water has relatively higher velocity and smaller depth, whereas a fluid with high viscosity like cement mortar or oil has relatively lower velocity and larger depth. The depth can be determined through preliminary placing for the same size of beam. The mean depth at the moment the flow front reaches the end of the form in the flow direction may be applied here. For the present study 100 mm was adopted as the depth.

The real aspects of the flow, when fresh UHPCC is placed, are of course more complex and quite different from the analytical solution: the flow in the initial condition is not fully developed and the flow front is dominated by fountain flow rather than shear flow. In addition, the flow shows different features near the end of the form after its front edge has arrived at the end, as there is no outlet.

However, until the flow front reaches the end of the form, the flow can be considered as shear flow. Furthermore, if it is assumed that the lower volume of the beam is filled before the flow reaches the end of the form and that the fiber orientation distribution is not influenced significantly by the different aspects of flow near the end, then the analytical result obtained with the assumption of a fully developed shear flow may not be substantially different from the actual results, considering that the fiber orientation distribution mainly influences the tensile behavior and the lower area in the beam is governed by the tensile stress.

The analyses were performed from the inlet to the mid-section of the beam. The number of streamlines is 18 and the flow distance is divided into 200 (see Fig. 3).

The variation of the fiber orientation distribution along the flow was computed with the help of the equation proposed by Folgar and Tucker [23], in which we neglected the interaction among fibers since no data on rotary diffusivity (D_r) is available that accounts for the interaction among fibers. Therefore the equation becomes the same with Jeffery's equation [20] as following equation.

$$\dot{p}_i = -\frac{1}{2}\omega_{ij}p_j + \frac{1}{2}\lambda(\dot{\gamma}_{ij}p_j - \dot{\gamma}_{kl}p_k p_l p_i) \quad (11)$$

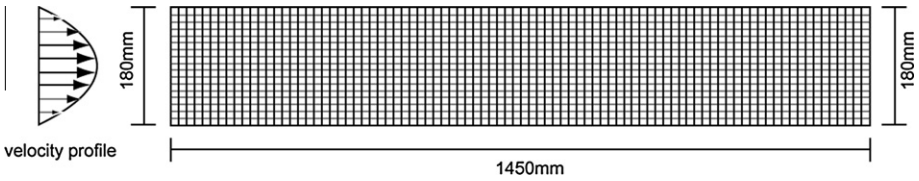

Fig. 3. Number of stream lines and flow distance lines.

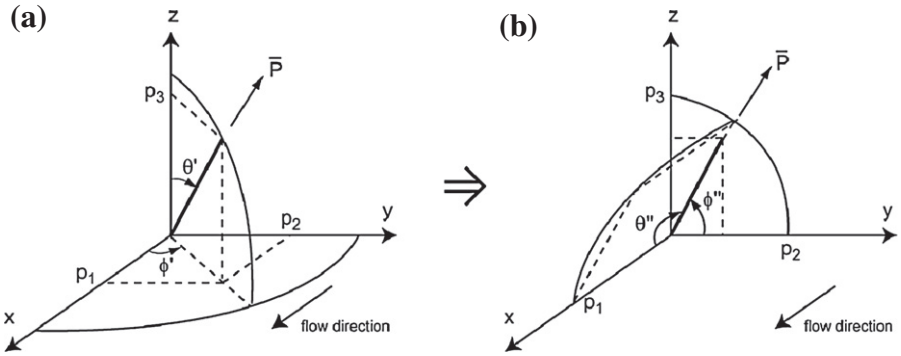

Fig. 4. Coordinate transformation: (a) before transformation, and (b) after transformation.

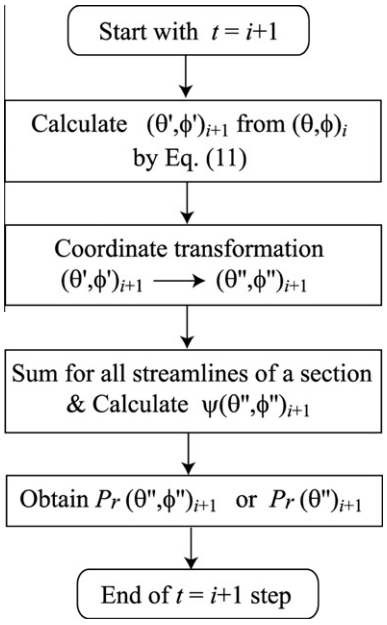

Fig. 5. Algorithm of the analysis.

3.2. Results of numerical analysis

For the three-dimensional fiber distribution, the following two equations can be obtained from Eqs. (1) and (11).

$$\frac{d\theta}{dt}=\frac{1}{2}\lambda\sin\theta\cos\theta\left\{2\left(\frac{\partial V_x}{\partial x}\right)\cos^2\phi+2\left(\frac{\partial V_y}{\partial x}+\frac{\partial V_x}{\partial y}\right)\cos\phi\sin\phi+2\left(\frac{\partial V_y}{\partial y}\right)\sin^2\phi\right\} \tag{12}$$

$$\frac{d\phi}{dt}=\cot\theta\cot\phi\left(\frac{d\theta}{dt}\right)+2\left(\frac{\partial V_y}{\partial x}-\frac{\partial V_x}{\partial y}\right)-\frac{\lambda}{2\sin\theta\sin\phi}\left\{2\left(\frac{\partial V_x}{\partial x}\right)\sin\theta\cos\phi+\left(\frac{\partial V_y}{\partial x}+\frac{\partial V_x}{\partial y}\right)\sin\theta\sin\phi\right\}+\frac{2\cot\phi}{\lambda}\left\{2\left(\frac{\partial V_x}{\partial x}\right)\sin^2\theta\cos^2\phi+2\left(\frac{\partial V_y}{\partial x}+\frac{\partial V_x}{\partial y}\right)\sin^2\theta\cos\phi\times\sin\phi+2\left(\frac{\partial V_y}{\partial y}\right)\sin^2\theta\sin^2\phi\right\} \tag{13}$$

Applying $V_y = V_z = 0$ in simple shear flow, Eqs. (12) and (13) can be reduced as

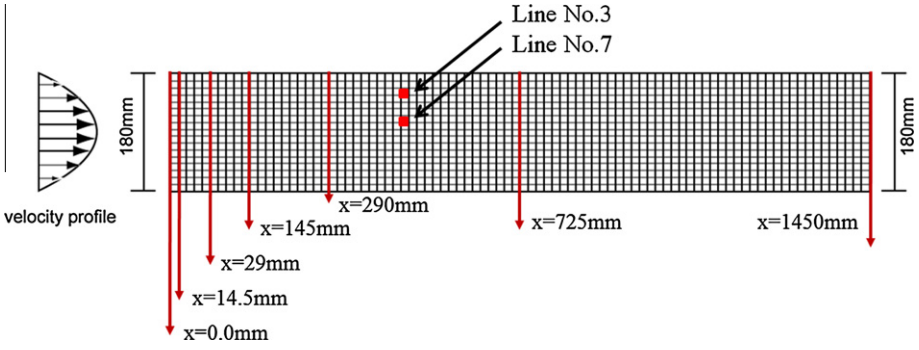

Fig. 6. Several flow distances and positions considered in the analysis.

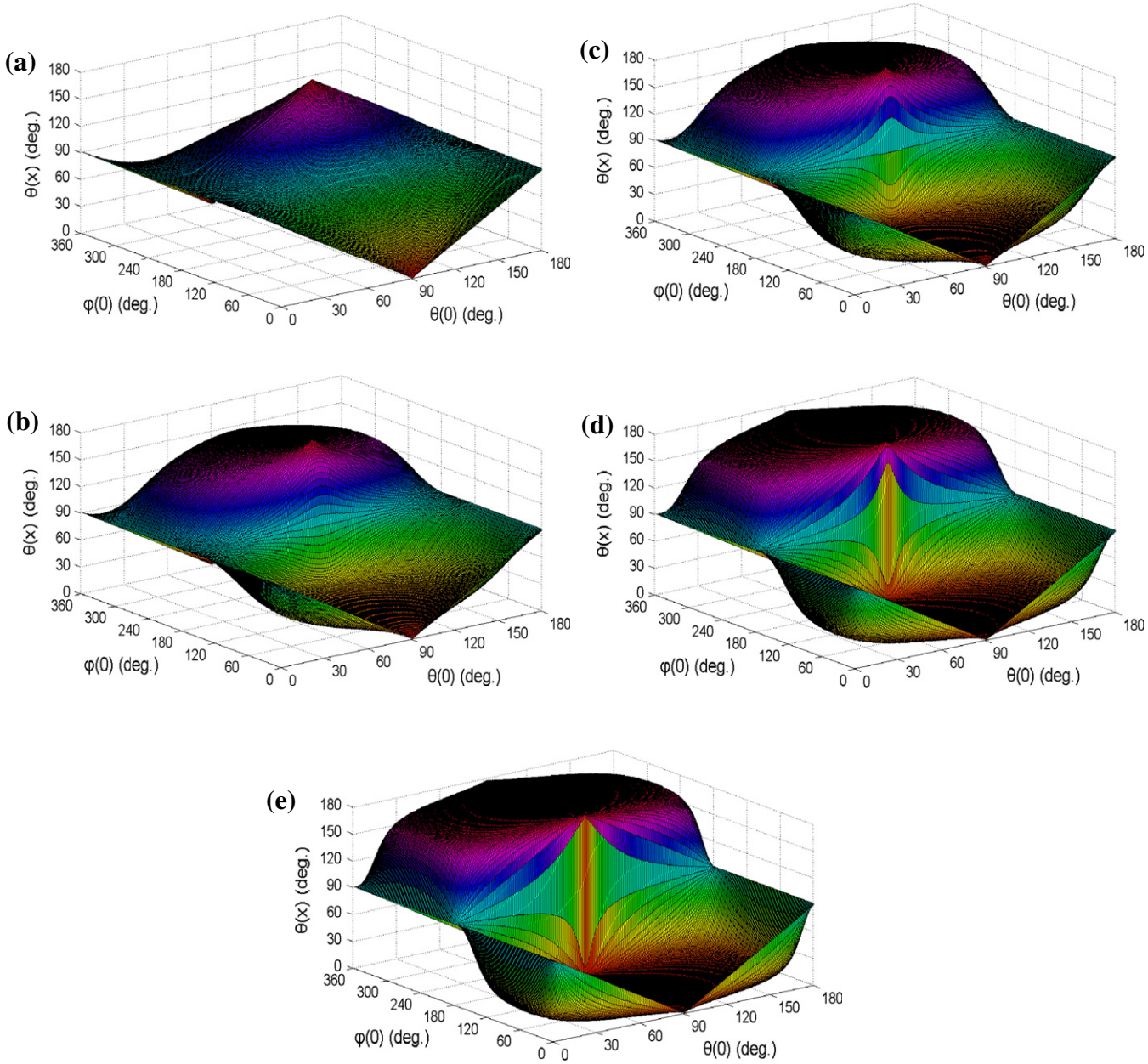

Fig. 7. Distributions of θ'' at different flow distances in line no. 3: (a) at x = 14.5 mm (b) at x = 145 mm (c) at x = 290 mm (d) at x = 725 mm (e) at x = 1450 mm.

$$\frac{d\theta}{dt} = \frac{1}{4}\lambda\left(\frac{\partial V_x}{\partial y}\right)\sin 2\theta\cos 2\phi \tag{14}$$

$$\frac{d\phi}{dt} = \left(\frac{\partial V_x}{\partial y}\right)\left(\lambda\cos^2\phi - \frac{1+\lambda}{2}\right) \tag{15}$$

When the initial fiber orientation is assumed to be uniformly distributed in three-dimensions, the distribution of (θ, ϕ) at a given time can be obtained by summation of the change of (θ, ϕ) for each time interval up to the time, which is calculated from Eqs. (14) and (15). The Probability Density Function (PDF) of (θ, ϕ) at each time step can be obtained using Eq. (10). The time step is dependent on the location in the section, and the maximum value was about 0.15 s near the wall.

In Eq. (10), however, θ' and ϕ' are defined in the coordinate system of Fig. 2. Therefore, in order to obtain PDF with respect to the flow direction, θ' and ϕ' must be transformed into the angles θ'' and ϕ'' with respect to the flow direction, as shown in Fig. 4.

Using θ'' and ϕ'' in the transformed coordinate system, PDF can be obtained as follows.

$$P_r(\theta'', \phi'', t) = \psi(\theta'', \phi'', t)\sin\theta d\theta d\phi \tag{16}$$

Fig. 5 illustrates the algorithm of the analysis. The analyses were performed at several sections illustrated in Fig. 6. Each section is at a distance of 1/100 (14.5 mm), 1/50 (29 mm), 1/10 (145 mm), 1/5 (290 mm), 1/2 (725 mm) of the total length, and 1450 mm, respectively. The orientation distribution of (θ, ϕ) was estimated in the positions presented in Fig. 6.

Especially, for the purpose of comparing the difference in fiber orientation distribution according to location in the same section, streamline No. 3 and No. 7 are considered. With the velocity profile of shear flow, streamline No. 3 has higher velocity gradient than No. 7. Fig. 7 shows the changed orientation distribution of the rotated angle θ'' at each position on streamline No.3, which is calculated from Eqs. (14) and (15). Fig. 8 presents the orientation distributions of θ'' about streamline No. 7. From Figs. 7 and 8,

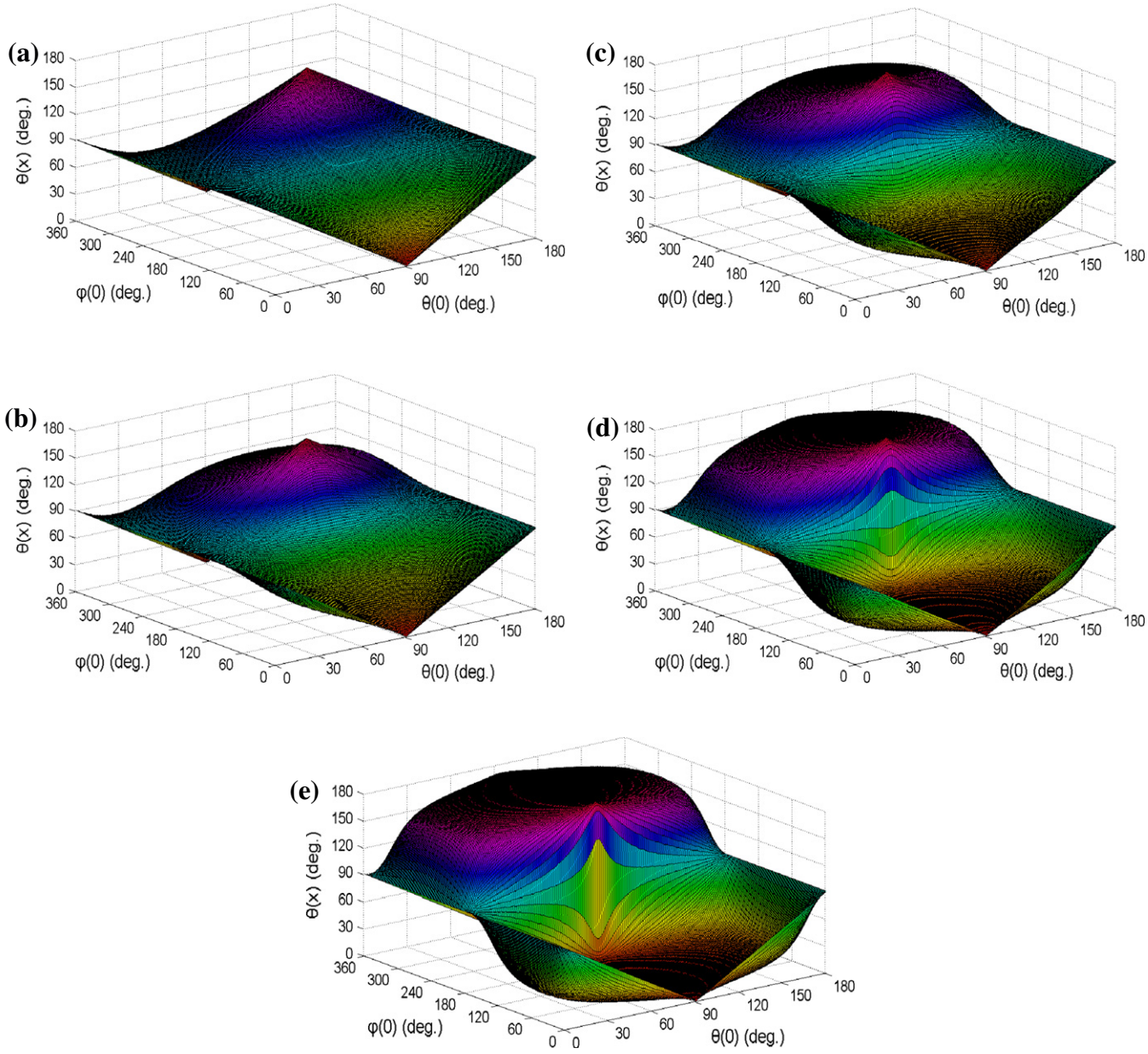

Fig. 8. Distributions of θ'' at different flow distances in line no. 7: (a) at x = 14.5 mm (b) at x = 145 mm (c) at x = 290 mm (d) at x = 725 mm (e) at x = 1450 mm.

it can be seen that most fibers with initial orientation of (θ, ϕ) gradually rotate toward 0° or 180° of θ'', and the rotational variation is faster in No. 3 than No. 7.

At a section, PDF of the inclined angle θ'' with respect to the flow direction can be obtained using the following equation.

$$P_r(\theta', t) = \int_{\phi=0}^{2\pi} \psi(\theta'', \phi'', t) \sin\theta \, d\theta \, d\phi \tag{17}$$

Fig. 9 presents the PDFs computed from Eq. (17) for different flow distances. From the results for the two-dimensional fiber distribution, it is found that the fibers seem to have a tendency to be arranged such that they gradually become more parallel to the flow direction as the flow distance increases. In particular, it is noted that initial distribution of θ experiences a tremendous rotational variation within just 72.5 mm flow distance, resulting in roughly inverse orientation distribution to the original.

4. Prediction of fiber orientation distribution in radial flow

4.1. Formulation of radial flow

Radial flow was also considered as another type of planar flow. The radial flow can be expressed using the cylindrical coordinate system. A suitable differential control volume for cylindrical coordinates is shown in Fig. 10.

For the incompressible flow in cylindrical coordinates, the governing equation can be expressed as following equation:

$$\frac{1}{r}\frac{\partial}{\partial r}(rV_r) + \frac{1}{r}\frac{\partial}{\partial \theta}V_\theta + \frac{\partial V_z}{\partial z} = 0 \tag{18}$$

Let us consider one-dimensional radial flow of $V_r = f(r)$ and $V_\theta = V_z = 0$ in the $r\theta$ plane. Eq. (18) reduces to the following equation.

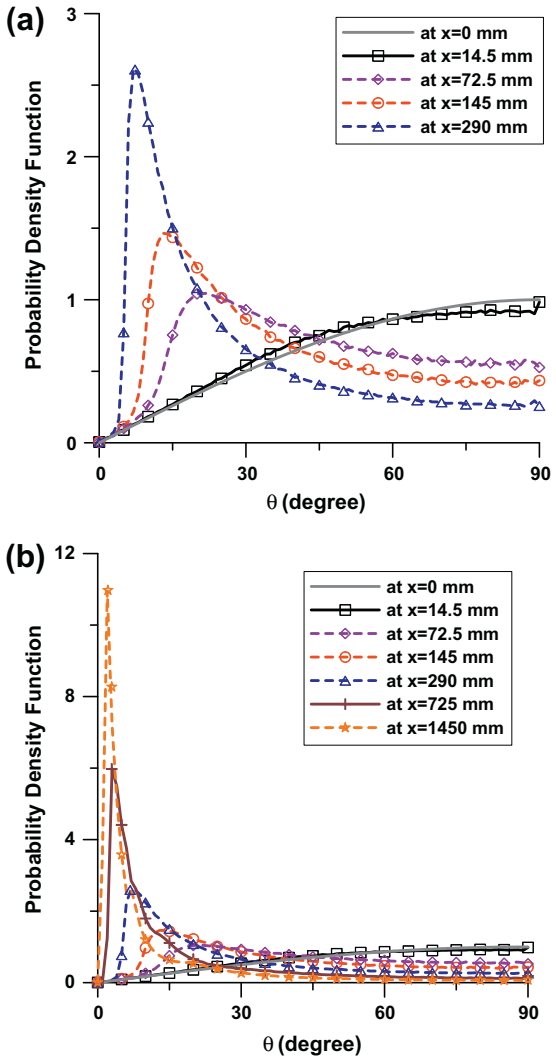

Fig. 9. Probability density functions of θ' at different flow distances (in shear flow).

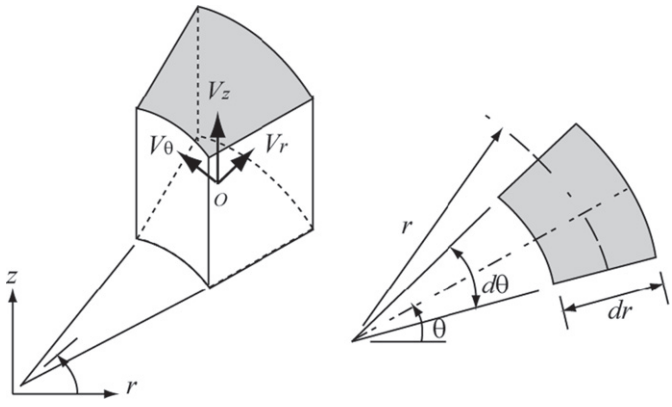

(a) isometric view (b) projection on $r\theta$ plane

Fig. 10. Differential control volume in cylindrical coordinates.

$$\frac{1}{r}\frac{\partial}{\partial r}(rV_r) = 0 \tag{19}$$

Integrating with respect to r gives

$$rV_r = \text{constant} \tag{20}$$

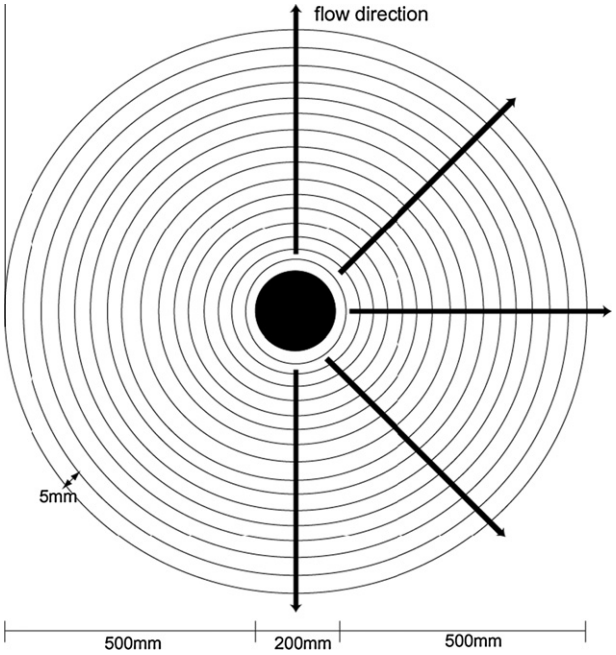

Fig. 11. Considered radial flow condition and flow step in analysis.

Thus it shows that the radial velocity must be $V_r = f(r) = C/r$ for one-dimensional radial flow of an incompressible fluid. That means, when Q is defined as the volume flow rate, as the fluid moves outwards from the center, the volume flow rate (per unit depth in the z direction) $Q = 2\pi r V_r$ at any radius r is constant.

For a given constant Q and h (the depth in the z direction), the radial velocity is expressed by

$$V_r = \frac{Q}{2\pi r h} \tag{21}$$

4.2. Analysis conditions

Here, we attempt to predict the variation of the fiber orientation distribution as the fresh UHPCC flows. In radial flow, there is only a radial velocity component. The flow volume rate in the inlet, Q was assumed to be 0.001 m^3/s. In addition, the flow depth was assumed to be 50 mm.

The analysis was performed under the assumption that UHPCC flows continuously with a constant rate of 0.001 m^3/s from a circular column with dimensions of 200 mm diameter and 50 mm height. The flow and the corresponding fiber orientation distribution were analyzed up to a radial flow distance of 600 mm from the center. The analysis interval in the flow direction (r direction) was 5 mm and thus there were a total of 100 steps (see Fig. 11).

The variation of the fiber orientation distribution along the flow was computed by Eq. (11), presented earlier.

4.3. Results of numerical analysis

For the three-dimensional fiber distribution, the following two equations can be obtained from Eqs. (1) and (11).

$$\frac{d\theta}{dt} = \frac{1}{2}\lambda\left(\frac{\partial V_r}{\partial r}\right)\sin 2\theta \cos^2\phi \tag{22}$$

$$\frac{d\phi}{dt} = -\lambda\left(\frac{\partial V_r}{\partial r}\right)\cot\phi \sin^2\phi \tag{23}$$

With the assumption that the initial fiber orientation is uniformly distributed in three-dimensions, the analysis was performed. For the points 100, 200, 300, 400, 500, 600 mm away from the center in Fig. 11, the fiber orientation distribution was obtained by analysis.

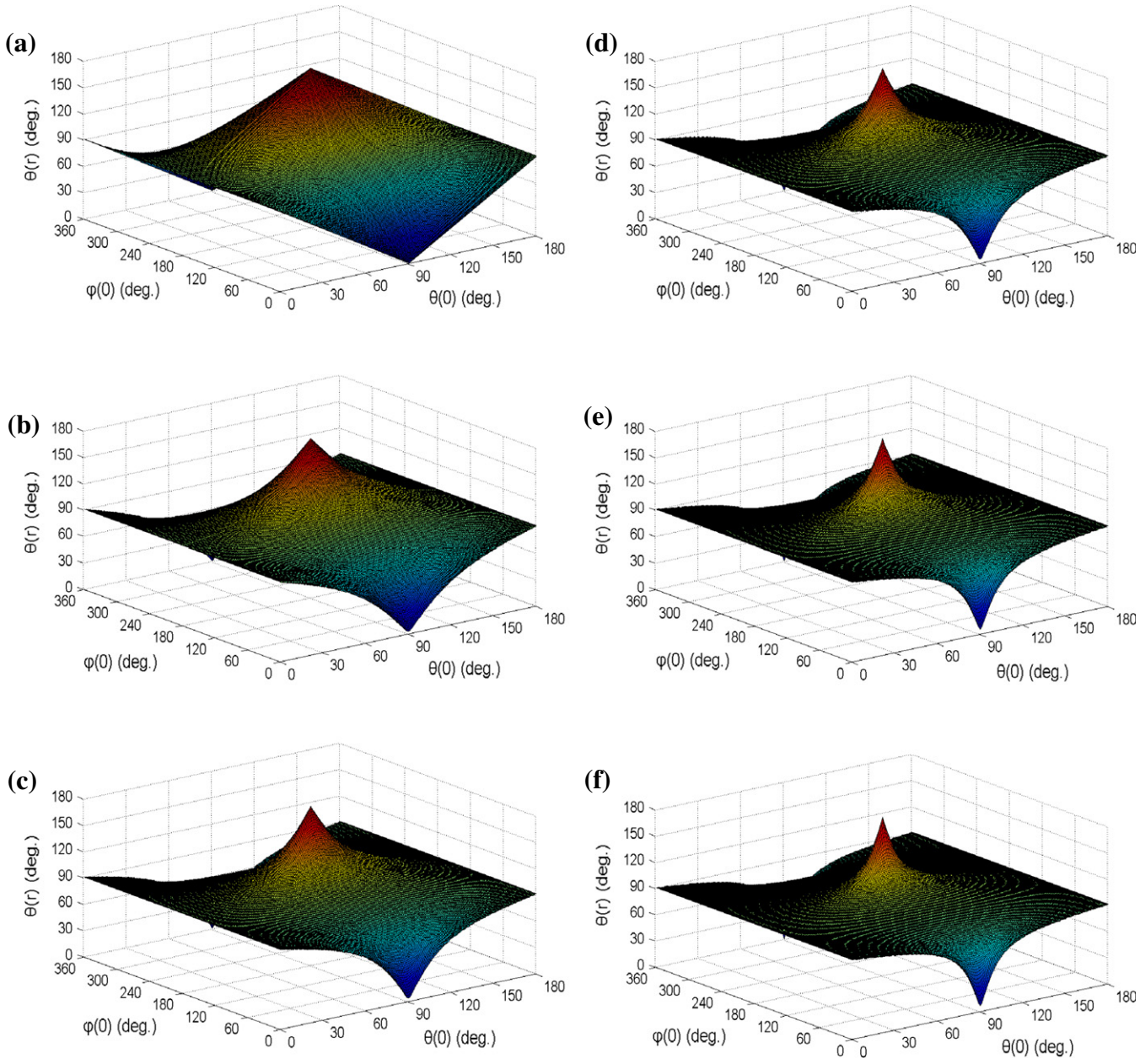

Fig. 12. Distributions of θ'' at different flow distances in radial flow: (a) at $r = 100$ mm (b) at $r = 200$ mm (c) at $r = 300$ mm (d) at $r = 400$ mm (e) at $r = 500$ mm (f) at $r = 600$ mm.

Fig. 12 shows the changed orientation distribution of the rotated angle θ'' at each point, which is the angle calculated from Eqs. (22) and (23), and then transformed with respect to the flow direction. Unlike in shear flow, Fig. 12 indicates that radial flow induces rotational movement of the randomly distributed fibers with (θ, ϕ) in initial condition toward 90° of θ''.

Fig. 13 presents PDFs at each location, obtained from Eq. (17) in a range of 0 to $\pi/2$. From Fig. 13, it is readily found that the fibers have a tendency to be arranged closer to perpendicular to the flow direction gradually as the flow distance increases.

For the radial flow, a previous experimental study [24] could be referred for comparison with the simulation. Even though it didn't provide quantitative estimation of fiber orientation distribution, but it could testify the trend of fiber rotational movement in radial flow of UHPCC through the obtained images of fiber distribution. The previous study [24] investigated the variation of the flexural behavior of UHPCC according to flow distance in radial flow. For the purpose, a thin plate of 1320 mm × 1320 mm × 100 mm was fabricated and divided into 36 pieces of small specimens for four-point bending test. In order to induce radial flow, fresh UHPCC was placed by free fall at the center of the plate, left to flow freely in the radial direction. Images of fiber distribution were obtained at the mid-section of all the bending test specimens. For comparison, mid-section images of three specimens at different locations were taken as shown in Fig. 14. Section 1 is very close to the circular area of the flow source, and Sections 2 and 3 are 220 mm and 440 mm away from Section 1 in the radial flow direction. Fig. 15 shows the fiber orientation distribution at each flow distance. The obtained images present the fiber orientation distribution on the surface normal to the radial flow direction. Considering the analytical result, it can be easily expected that fiber distribution in the image changes from a distribution close to initial condition into a distri-

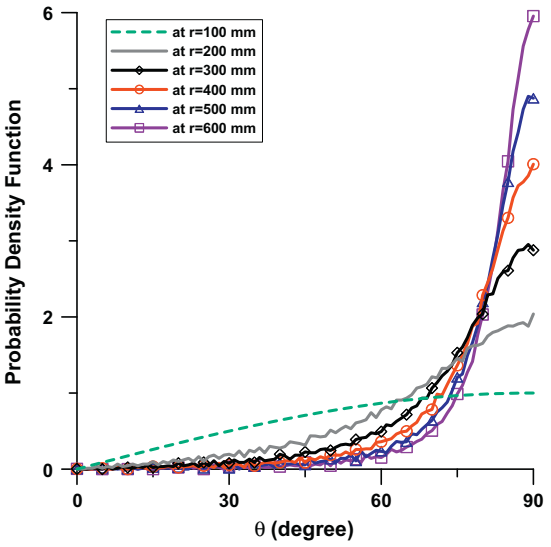

Fig. 13. Probability density functions of θ'' at different flow distances (in radial flow).

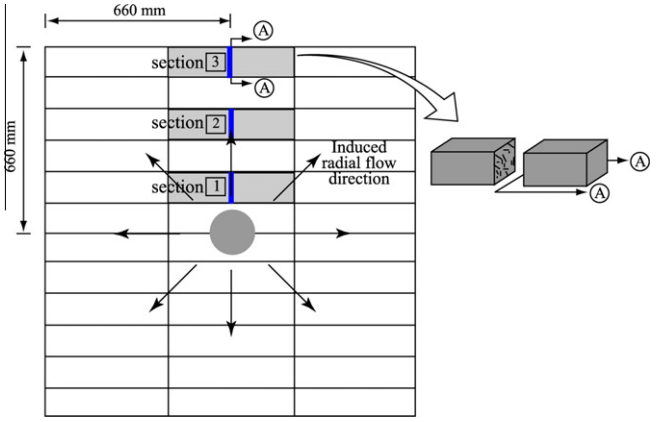

Fig. 14. Inducement of radial flow in fabricating UHPCC plate and cut bending specimens taken for images of fiber orientation distribution.

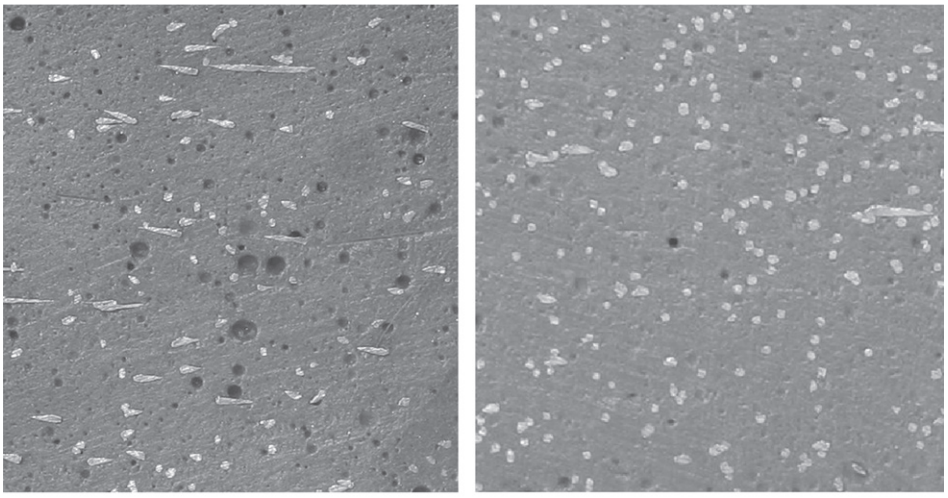

(a) at section 1 (b) at section 2

(c) at section 3

Fig. 15. Comparison of fiber distribution images at different flow distances in radial flow of UHPCC.

bution that all fibers are almost aligned perpendicularly to the cut plane as the radial flow proceeds. This tendency can be found in Fig. 15, which demonstrates the variation of fiber orientation distribution in radial flow of UHPCC. The comparison in Fig. 15 is not directly correlated with the analytical result on quantitative basis, but at least it shows the legitimacy of the analytical approach of this study.

5. Conclusions

In this paper, the variation of the fiber orientation distribution during flow molding of UHPCC was studied. In order to describe the rotational motion of a single fiber, Jeffery's equation was adopted, in which the interaction among fibers is neglected. The fiber orientation distribution along the flow distance was estimated with the assumption of 3-dimensional random distribution at the beginning of flow.

Assuming that the flow is a fully developed shear flow between infinite parallel plates in a steady state, prediction of the variation of the fiber orientation distribution in shear flow was implemented. Analytical results revealed that the fibers have a tendency to be arranged such that they gradually become more parallel to the flow direction as the flow distance increases.

Prediction of the variation of fiber orientation distribution in radial flow was also performed. The analysis demonstrated that the fibers have a tendency to be arranged such that they gradually become more perpendicular to the flow direction as the flow distance increases. This tendency was verified by comparing with a previous experimental study.

Flow-dependent fiber orientation analysis was implemented, neglecting the interaction among fibers for simplicity, but interactions might occur particularly for high volume fractions of fibers (e.g. 2 vol.% or more). Further research is necessary to study the effects of such fiber interaction. This study supports the prediction of flow-dependent tensile behavior, considering changes in the fiber orientation distribution, and the achievement of more reliable design and construction of structures utilizing UHPCC.

References

[1] Richard P, Cheyrezy M. Composition of reactive powder concretes. Cem Concr Res 1995;25(7):1501–11.
[2] Stahli P, Custer R, van Mier JGM. On flow properties, fiber distribution, fiber orientation and flexural behavior of FRC. Mater Struct 2008;41(1):189–96.
[3] Kang ST, Lee BY, Kim JK, Kim YY. The effect of fibre distribution characteristics on the flexural strength of steel fibre-reinforced ultra high strength concrete. Constr Build Mater 2011;25(5):2450–7.
[4] Ferrara L, di Prisco M, Lamperti MGL. Identification of the stress-crack opening behavior of HPFRCC: the role of flow-induced fiber orientation. In: Proceeding of the 7th international conference on fracture mechanics of concrete and concrete structures (FraMCos-7). Jeju: 2010. p. 1541–50.
[5] Shah SP, Ouyang C. Mechanical behavior of fiber-reinforced cement-based composites. J Am Ceram Soc 1991;74(11):2727–38.
[6] Naaman AE, Reinhardt HW. Characterization of high performance fiber reinforced cement composites-HPFRCC. In: Proceedings of the second international workshop 'HPFRCC2'; 1995. p. 3–6.
[7] Akkaya Y, Picka J, Shah SP. Spatial distribution of aligned short fibers in cement composites. ASCE J Mater Civ Eng 2000;12(3):272–9.
[8] Poitou A, Chinesta F, Bernier G. Orienting fibers by extrusion in reinforced reactive powder concrete. J Eng Mech 2001;127(6):593–8.
[9] Petit J-Y, Wirquin E, Khayat KH. Effect of temperature on the rheology of flowable mortars. Cem Concr Compos 2010;32(1):43–53.
[10] Leemann A, Winnefeld F. The effect of viscosity modifying agents on mortar and concrete. Cem Concr Compos 2007;29(5):341–9.
[11] Batchelor GK. Slender-body theory for particles of arbitrary cross section in stokes flow. J Fluid Mech 1970;44:419–40.
[12] Ausias G, Agassant JF, Vincent M. Rheology of short glass fiber reinforced polypropylene. J Rheol 1992;36(4):525–43.
[13] Advani SG. Flow and rheology in polymer composites manufacturing. Amsterdam: Elsevier Science; 1994.
[14] Vincent M, Delivers E, Agassant JF. Fiber orientation calculation in injection moulding of reinforced thermoplastics. J Non-Newton Fluid Mech 1997;73:317–26.
[15] Chiba K, Nakamura K. Numerical solution of fiber suspension flow through a complex channel. J Non-Newton Fluid Mech 1998;78:167–85.
[16] Chiba K, Yasuda K, Nakamura K. Numerical solution of fiber suspension flow through a parallel plate channel by coupling flow field with fiber orientation distribution. J Non-Newton Fluid Mech 2001;99:145–7.
[17] Moses KB, Advani SG, Reinhardt A. Investigation of fiber motion near solid boundaries in simple shear flow. Rheol Acta 2001;40:296–306.
[18] Han KH, Im YT. Numerical simulation of three-dimensional fiber orientation in short-fiber-reinforced injection-molded parts. J Mater Process Technol 2002;124:366–71.
[19] Lin JZ, Sun K, Zhang W. Orientation distribution of fibers and rheological property in fiber suspensions flowing in a turbulent boundary layer. Acta Mech Sinica 2008;24:243–50.
[20] Jeffery GB. The motion of ellipsoidal particles immersed in a viscous fluid. Proc Roy Soc London 1922;A102:161–79.
[21] Dinh SM, Armstrong RC. A rheological equation of state for semiconcentrated fiber suspensions. J Rheol 1984;28:207–27.
[22] Folgar F, Tucker III CL. Orientation behavior of fibers in concentrated suspensions. J Reinf Plast Compos 1984;3:98–119.
[23] Advani SG, Tucker III CL. The use of tensor to describe and predict fiber orientation in short fiber composites. J Rheol 1987;31(8):751–84.
[24] Kang ST, Park JJ, Ryu GS, Kim SW. Investigation of fiber alignment of UHSFRC in flexural members. In: Proceedings of 8th international symposium on utilization of high-strength and high-performance concrete. Tokyo: 2008. p. 709–14.